Insight into the Photophysics of Dual Strong Emission (Blue & Green) Producing Graphene Quantum Dot Clusters and their Application Towards Selective and Sensitive Detection of Trace Level Fe^{3+} and Cr^{6+} Ions

Ganapathi Bharathi[1#], Devaraj Nataraj[1,2*], Sellan Premkumar[1$], Padmanaban Saravanan[3], Daniel T. Thangadurai[4], Oleg Yu Khyzhun[5], Kittusamy Senthilkumar[2,6], Ramasamy kathiresan[7], Ponmalai Kolandaivel[7,9], Mukul Gupta[8], Deodatta Phase[8]

1 Quantum Materials & Energy Devices (QM-ED) Laboratory, Department of Physics, Bharathiar University, Coimbatore, TN, India
2 UGC- CPEPA Centre for Advanced Studies in Physics for the development of Solar Energy Materials and Devices, Department of Physics, Bharathiar University, Coimbatore, TN, India
3 Defence Metallurgical Research Laboratory, Hyderabad 500 058, India
4 Department of Nanoscience and Technology, Sri Ramakrishana Engineering College, Affiliated to Anna University, Coimbatore – 641 022, TN, India.
5 Department of Structural Chemistry of Solids, Frantsevych Institute for Problems of Materials Science, National Academy of Sciences of Ukraine, UA-03142 Kyiv, Ukraine
6 Department of Physics, Bharathiar University, Coimbatore, TN, India
7 Macromolecular Laboratory, Department of Physics, Bharathiar University, Coimbatore, TN, India
8 UGC-DAE Consortium for Scientific Research, Indore, MP, India
9 periyar University, Salem, TN, India
*** de.natraj2011@gmail.com**

Present address: Key Laboratory of Optoelectronic Devices and Systems of Guangdong Province, College of Optoelectronic Engineering, Shenzhen University, Shenzhen, Guangdong Province, 518060 P.R. China

$ Present address: School of Chemistry and Chemical Engineering, Tianjin Polytechnic University, Tianjin, 300387, China, and School of Material Science and Engineering, Tianjin Polytechnic University, Tianjin, 300387, China

Supporting information:

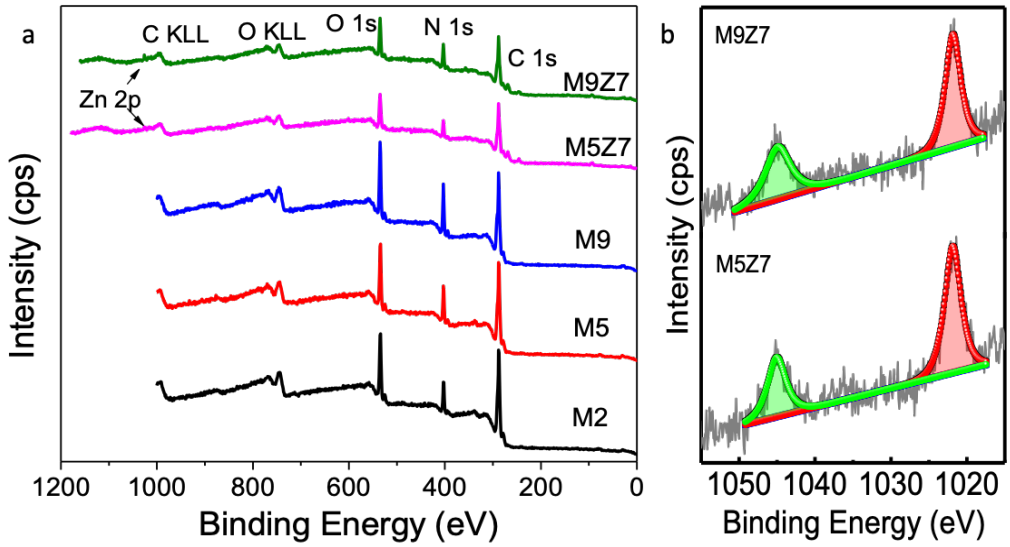

Figure S1. XPS survey spectra of GQDs (M2, M5 and M9) and GQD interconnected wire-like network samples (M5Z7 and M9Z7). The GQD samples show the presence of carbon, nitrogen and oxygen, and the GQD interconnected wire-like network samples indicate the additional presence of zinc, which was responsible for the wire-like nanostructure formation. The Zn 2p spectra of M5Z7 and M9Z7 samples indicate two distinct peaks at 1022.1 eV and 1044.2 eV, which correspond to Zn $2p_{3/2}$ and Zn $2p_{1/2}$ components, thereby confirming the presence of Zn metal atoms in the GQD interconnected wire-like network samples.[1]

Table T1. Elemental content of the GQDs (M2-M9) and GQD interconnected wire-like network (M5Z7 and M9Z7) samples (at.%)

Sample	**C**	**N**	**O**	**Zn**
M2	72.1	12.2	15.7	-
M5	64.1	16.8	19.1	-
M9	65.6	17.4	17.0	-
M5Z7	75.5	11.1	13.1	0.3
M9Z7	75.3	12.6	11.80	0.3

C-Carbon, N-Nitrogen, O-Oxygen, Zn-Zinc

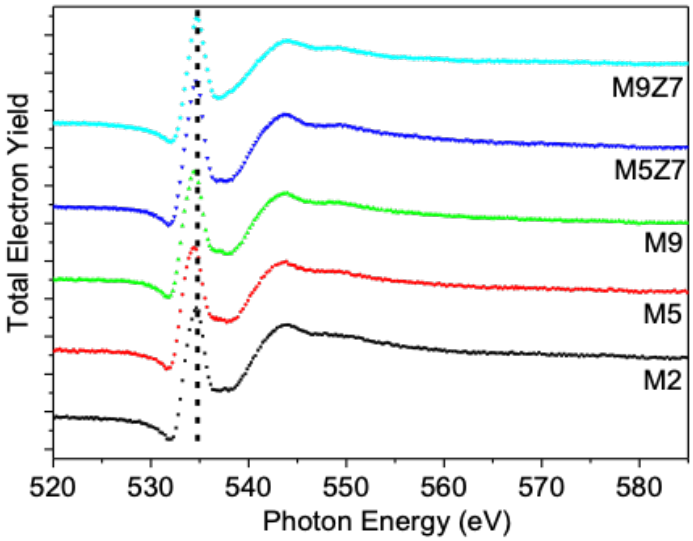

Figure S2. O 1s X-ray absorption spectra (XAS) of GQDs (M2, M5 and M9) and GQD interconnected wire-like network (M5Z7 and M9Z7) samples. The O 1s XAS spectra display a sharp peak at 534.2 eV corresponding to 1s-π* transition of C=O in all the as prepared samples. In addition, the broad band beyond 540 eV is the superposition of 1s-σ* transitions of C-O and C=O.[2,3]

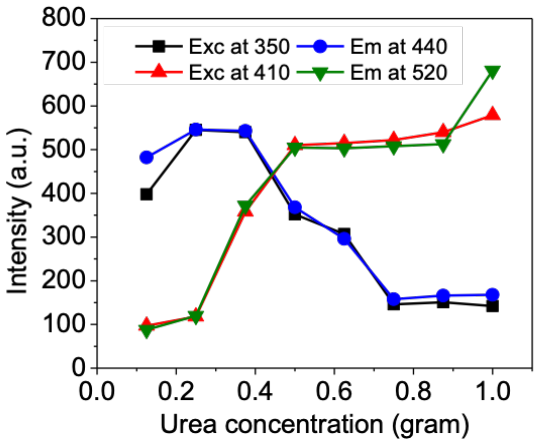

Figure S3. Relation between urea concentration and blue/green excitation/emission. As the urea concentration increases, the blue excitation/emission intensities decrease and the green excitation/emission intensities increase. This indicates the role of urea in tuning the emission maxima to either blue (440 nm) or green (520 nm).

Table T2. Quantum yield values for blue and green emissions corresponding to the GQDs and GQD coupled solid structures

Emission/samples	**M2**	**M5**	**M9**	**M5Z7**	**M9Z7**
Blue	18%	16%	6%	18%	15%
Green	2%	19%	18%	16%	19%

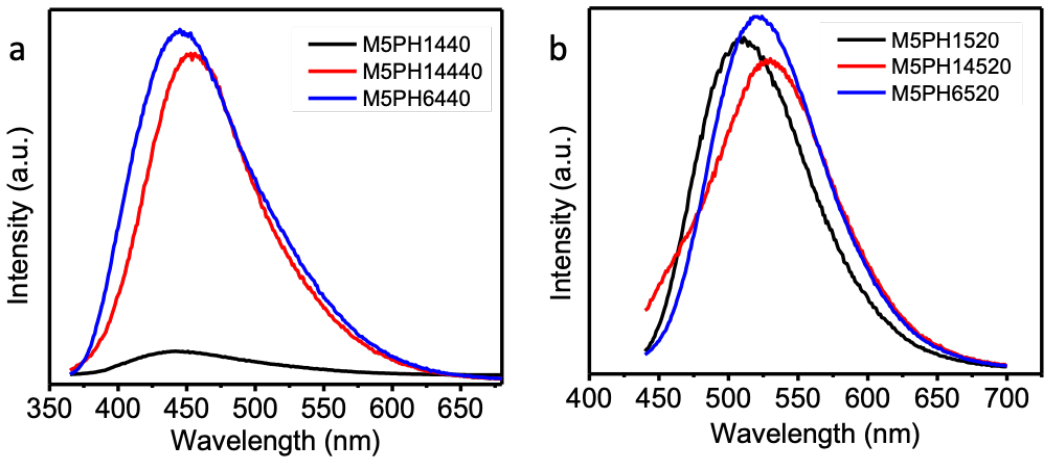

Figure S4. pH dependent PL Emission spectra of the M5 sample, measured at (a) Blue (440 nm) and (b) Green (520 nm) emission positions. The pH dependent PL study indicates that the blue emission is pH dependent and the green emission is pH independent. When the pH was reduced to 1, the blue emission was quenched to a minimum value and the emission was retained almost to its original value upon increasing the pH to 14. This effect is caused by the deprotonation – re-protonation of the carboxyl functional groups. The major part of the blue emission is contributed by the surface states and functional groups. The green emission is originating from the sp2 domains containing a greater number of nitrogen species.

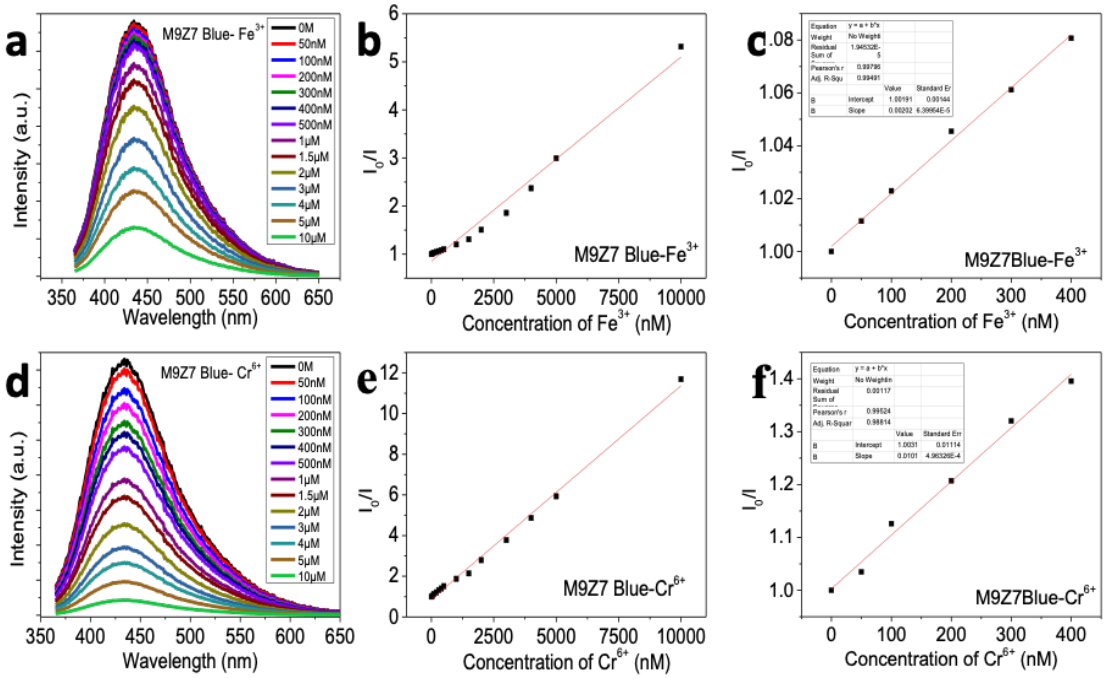

Figure S5. (a), (d) PL spectra of M9Z7 blue emission, showing the PL quenching upon addition of Fe^{3+} and Cr^{6+} ions, respectively; (b), (e) Stern-Volmer plots showing the linear response of M9Z7 blue emission up to 10 μM, against Fe^{3+} and Cr^{6+} ions, respectively; (c), (f) Stern-Volmer plots for the concentration up to 400 nM, which were used to calculated the quenching constants and limit of detection (LoD) values for the addition of Fe^{3+} and Cr^{6+} analytes, respectively.

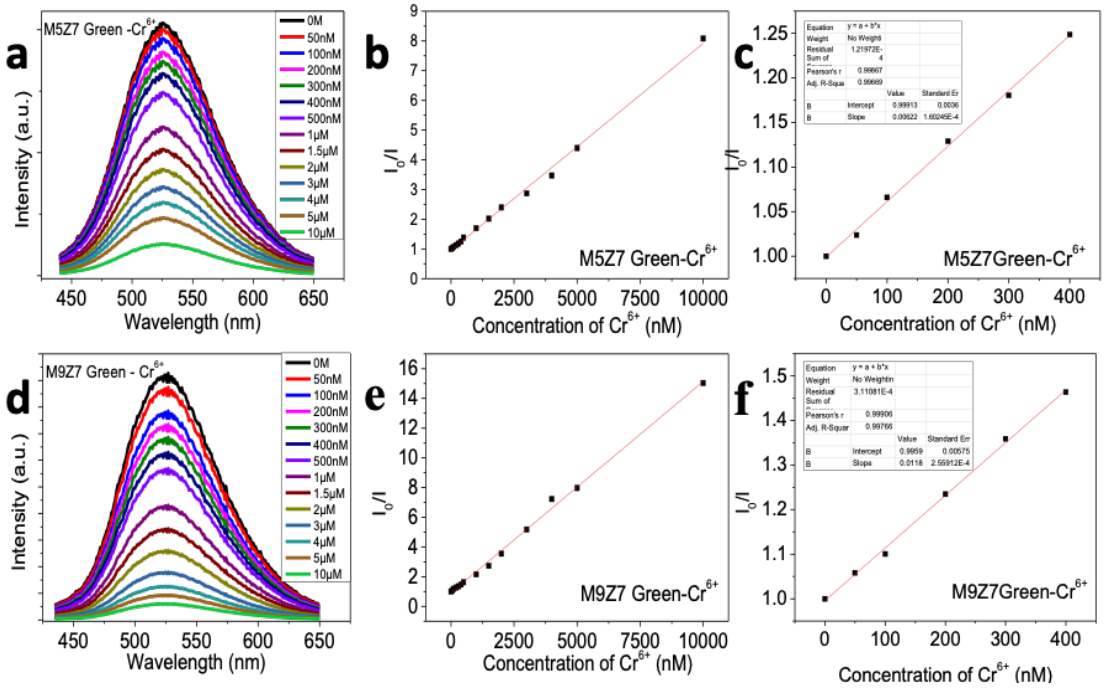

Figure S6. PL spectra of (a) M5Z7 green and (d) M9Z7 green emissions, showing the PL quenching upon addition of Cr^{6+} ions; (b), (e) Stern-Volmer plots showing the linear response of M5Z7 green and M9Z7 green up to 10 μM, against and Cr^{6+} ions; (c), (f) Stern-Volmer plots for the concentration up to 400 nM, which were used to calculated the quenching constants and limit of detection (LoD) values for the addition of Cr^{6+} analytes.

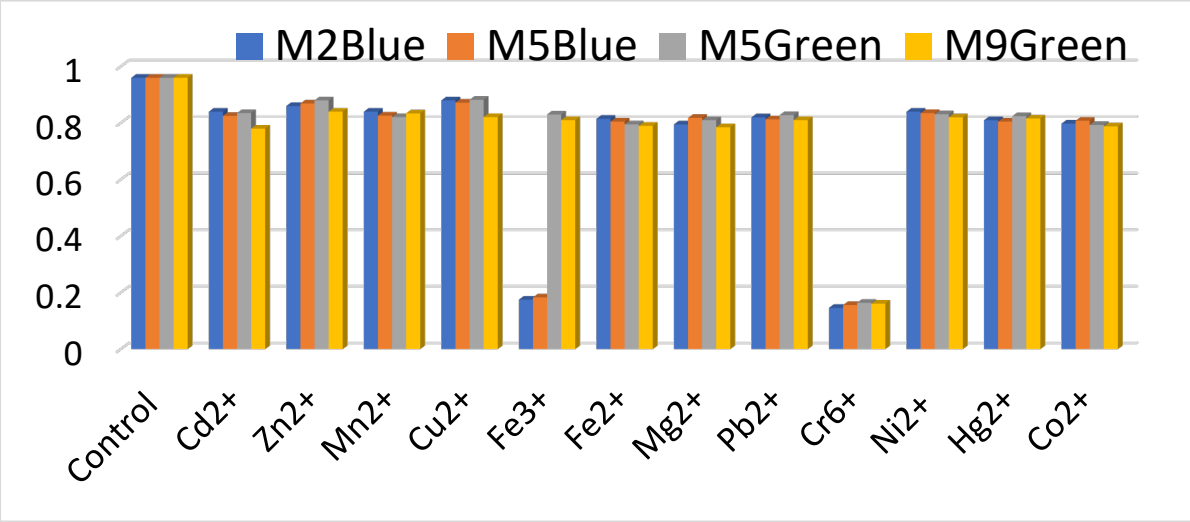

Figure S7. Bar chart showing the selectivity of GQD samples against Fe^{3+} and Cr^{6+} ions. The samples were able to detect Fe^{3+} and Cr^{6+} ions selectively. The blue emission was quenched by both Fe^{3+} and Cr^{6+} ions, and the green emission was quenched only by Cr^{6+} ions.

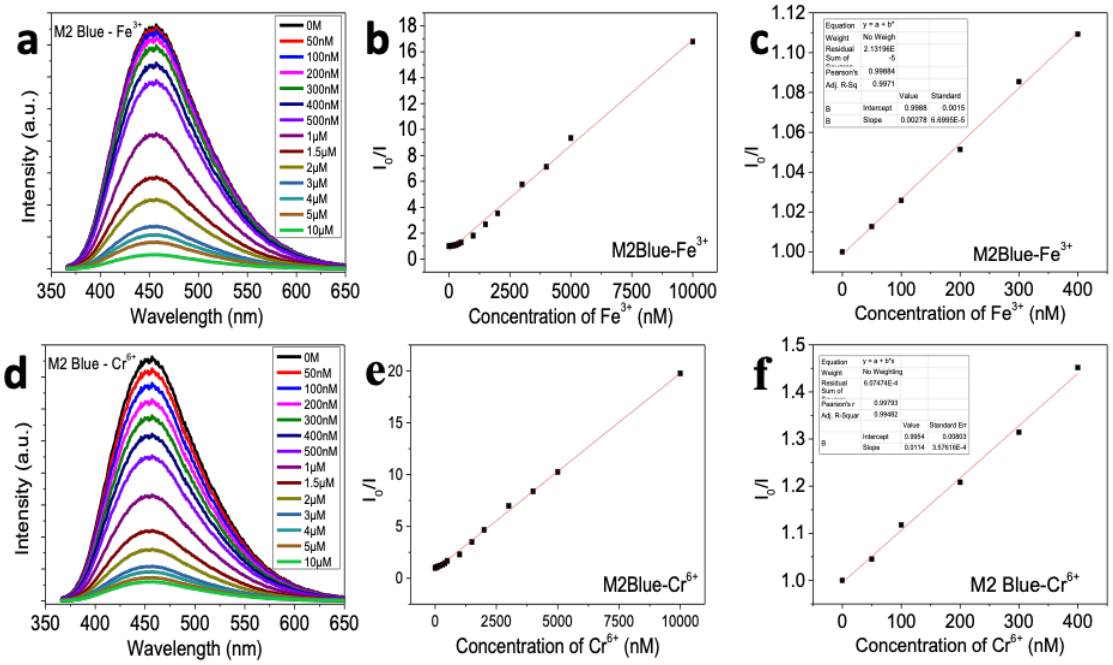

Figure S8. (a), (d) PL spectra of M2 blue emission, showing the PL quenching upon addition of Fe^{3+} and Cr^{6+} ions, respectively; (b), (e) Stern-Volmer plots showing the linear response of M2 blue emission up to 10 μM, against Fe^{3+} and Cr^{6+} ions, respectively; (c), (f) Stern-Volmer plots for the concentration up to 400 nM, which were used to calculated the quenching constants and limit of detection (LoD) values for the addition of Fe^{3+} and Cr^{6+} analytes, respectively.

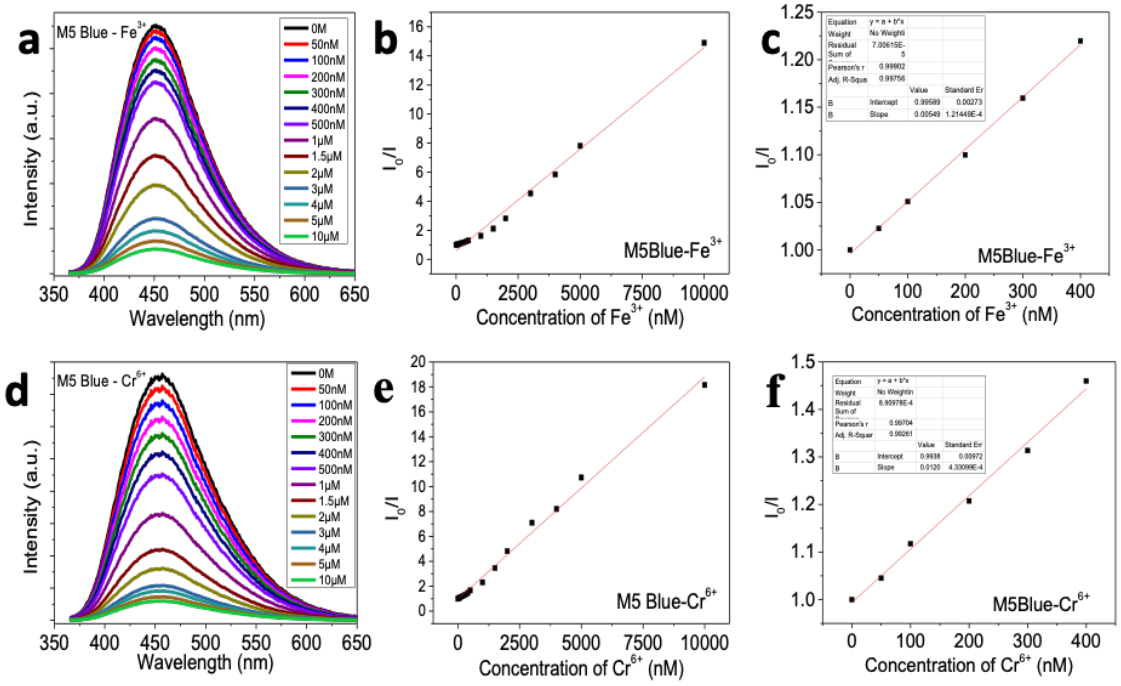

Figure S9. (a), (d) PL spectra of M5 blue emission, showing the PL quenching upon addition of Fe^{3+} and Cr^{6+} ions, respectively; (b), (e) Stern-Volmer plots showing the linear response of M5 blue emission up to 10 μM, against Fe^{3+} and Cr^{6+} ions, respectively; (c), (f) Stern-Volmer plots for the concentration up to 400 nM, which were used to calculated the quenching constants and limit of detection (LoD) values for the addition of Fe^{3+} and Cr^{6+} analytes, respectively.

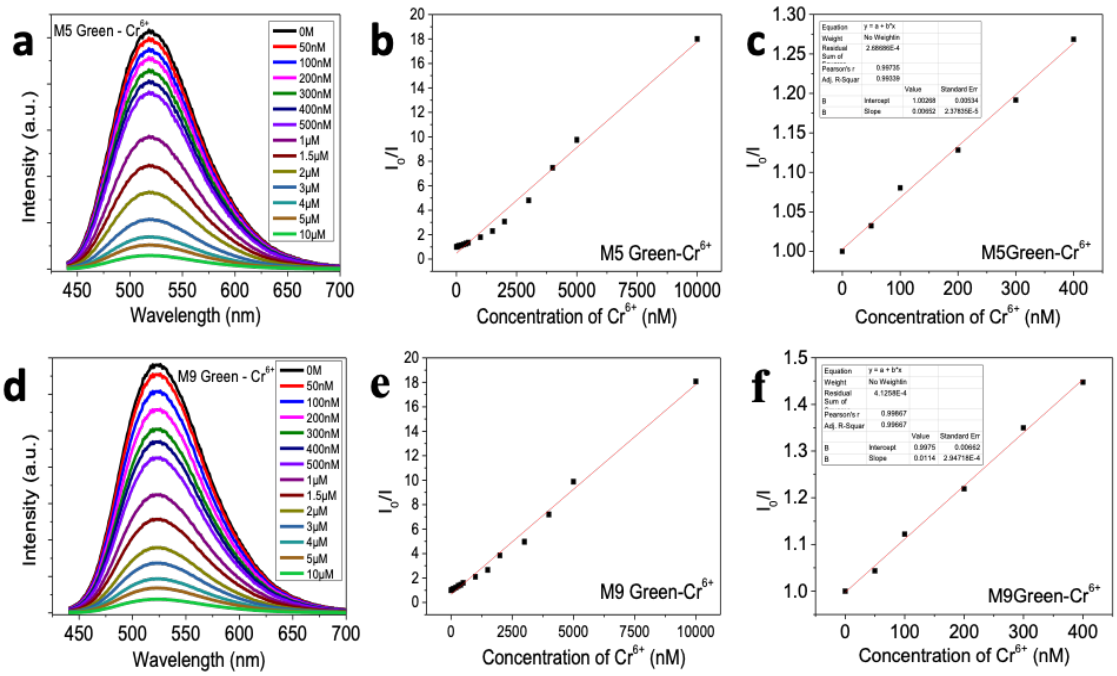

Figure S10. PL spectra of (a) M5 green and (d) M9 green emissions, showing the PL quenching upon addition of Cr^{6+} ions; (b), (e) Stern-Volmer plots showing the linear response of M5 green and M9 green up to 10 μM, against and Cr^{6+} ions; (c), (f) Stern-Volmer plots for the concentration up to 400 nM, which were used to calculated the quenching constants and limit of detection (LoD) values for the addition of and Cr^{6+} analytes.

Table T3. Comparison of present results with literature (Fe^{3+} - iron ion)

Probe	Analyte	Detection range	Detection limit	Reference
Carbon dots	Fe^{3+}	0.02 – 40 μM	0.13 μM	[4]
Carbon dots	Fe^{3+}	1 – 100 μM	0.32 μM	[5]
Nitrogen doped carbon dots	Fe^{3+}	0.01 μM – 450 μM	0.005 μM	[6]
nitrogen and phosphor co-doped carbon quantum dots	Fe^{3+}	0.05 –200 μM	0.05 μM	[7]
nitrogen and sulfur co-doped Carbon dots	Fe^{3+}	1.56 –200 μM	12.5 nM	[8]
Self-doped Carbon dots	Fe^{3+}	0 to 1.6 μM	0.05 μM	[9]
Nitrogen doped Carbon dots	Fe^{3+}	0 – 500 μM	70 μM	[10]
Carbon dots	Fe^{3+}	25-300 μM	19 μM	[11]
Nitrogen doped graphene quantum dots	Fe^{3+}	1–70 μM	0.08 μM	[12]
Rhodamine-Functionalized Graphene Quantum Dots	Fe^{3+}	0 to 65 μM	0.02 μM	[13]
graphene quantum dots	Fe^{3+}	1.0–400 μM	7.22 μ M	[14]
GQD wire-like Nanoclusters	Fe^{3+}	0-10 μM	43 nM	Present work

Table T4. Comparison of present results with literature (Cr^{6+} - Chromium ion)

Probe	Analyte	Detection range	Detection limit	Reference
Carbon dots	Cr^{6+}	1.0–400 μM	0.24 μM	[15]
graphene nanosheets	Cr^{6+}	0−20 mM	0.51 μM	[16]
Carbon dots	Cr^{6+}	0.52− 2600 μg/L	50 μg/L	[17]
Graphene quantum dots	Cr^{6+}	0.05 to 500 μM	3.7 nM	[18]
GQD wire-like Nanoclusters	Cr^{6+}	0-10 μM	43 nM	Present work

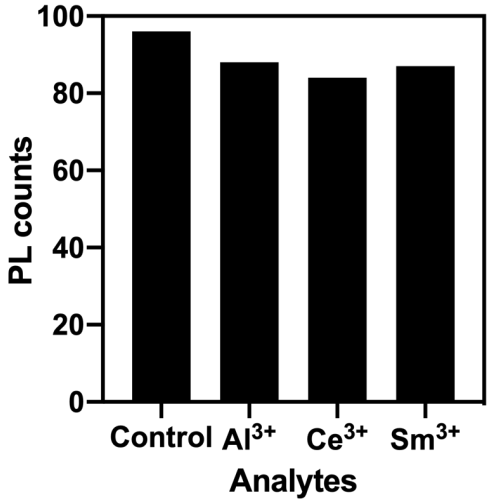

Figure S11. Bar chart showing the response of GQD nanostructured probe (M5 sample) against tripositive metal ions. The sample's PL emission remain unaffected against these metal ions.

The sensing experiments were extended to investigate the response of GQD nanostructured probes against tripositive metal ions, such as Al^{3+}, Ce^{3+} and Sm^{3+}. The experimental results reveal that, our GQD nanostructures do not respond to the tripositive metal ions, i.e., the PL emission of our GQD nanostructured probes remain unaffected upon addition of these metal ions. This indicate a fact that our GQD nanostructured probes are highly selective towards Fe^{3+} and Cr^{6+} ions.

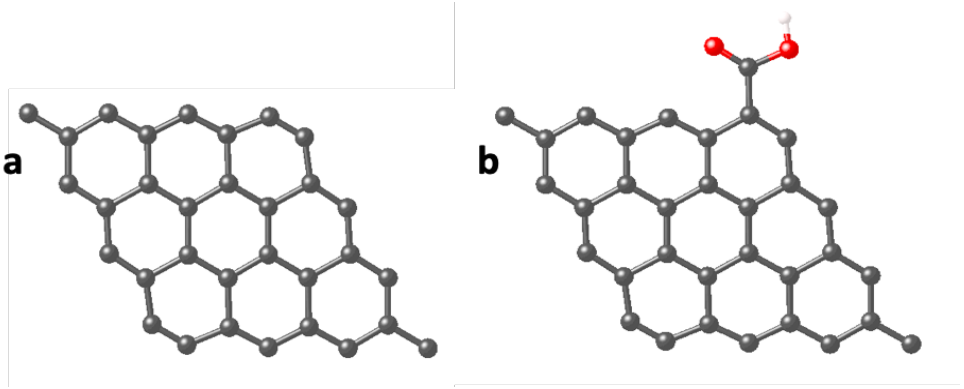

Figure S12. Optimized structure of (a) GQD and (b) COOH functionalized GQD. The carbon, oxygen and hydrogen atoms are black, red, and pink in color, respectively.

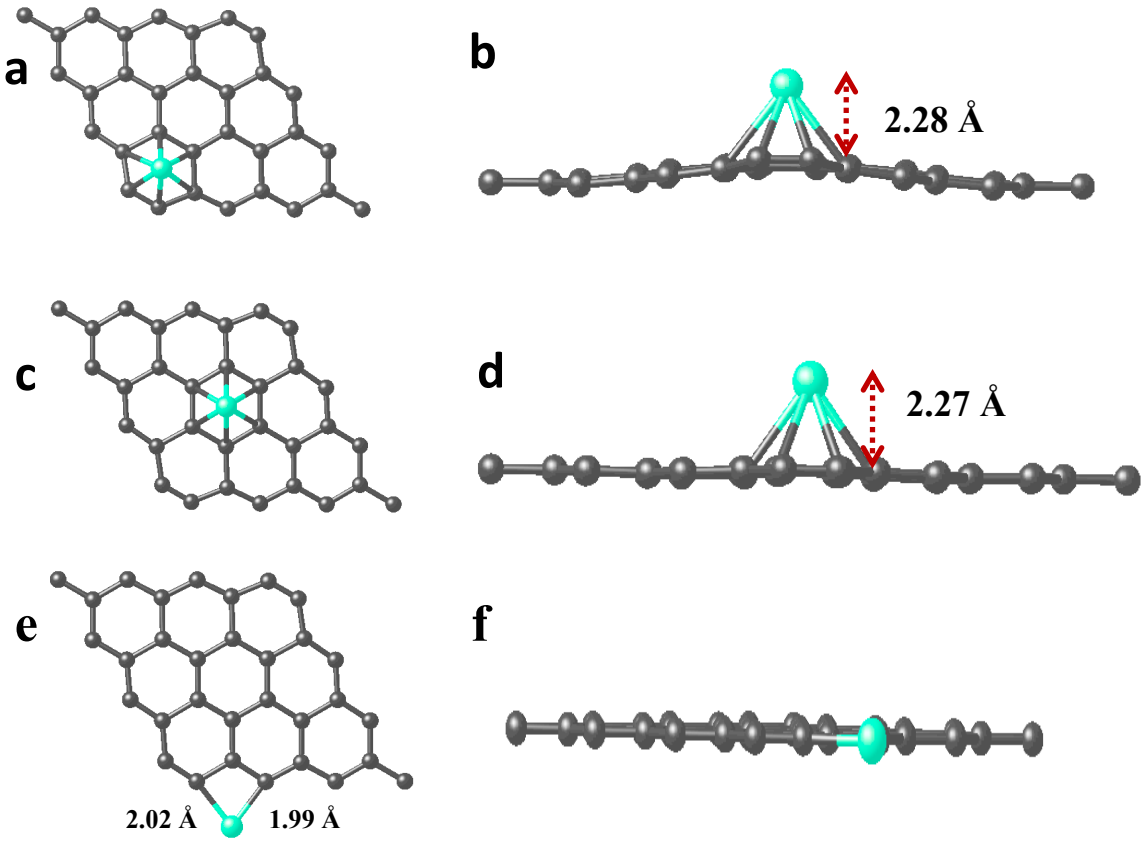

Figure S13. Optimized structure of GQD-Fe^{3+} complex, (a) bridge-hollow (BH) configuration, (c) hollow-hollow (HH) configuration and (e) Edge-Edge (EE) configuration. (b), (d) & (f) are the side views of the optimized structures presented in (a), (c) & (e), respectively. The carbon and Fe^{3+} ion are black and green in color, respectively.

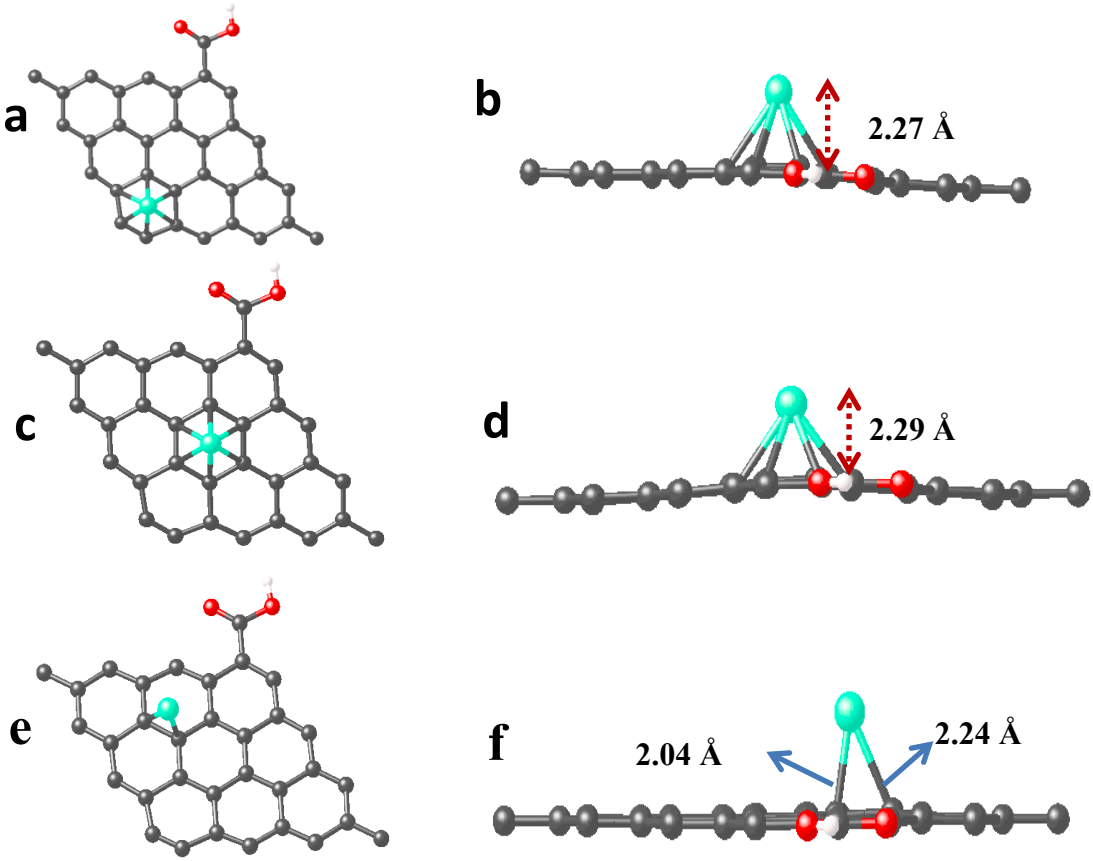

Figure S14. Optimized structure of COOH functionalized GQD-Fe complex, (a) bridge-hollow (BH) configuration, (c) hollow-hollow (HH) configuration and (e) Top-bridge (TB) configuration. (b), (d) & (f) are the side views of the optimized structures presented in (a), (c) & (e), respectively. The carbon, oxygen, hydrogen atoms and Fe^{3+} ion are black, red, pink and green in color, respectively.

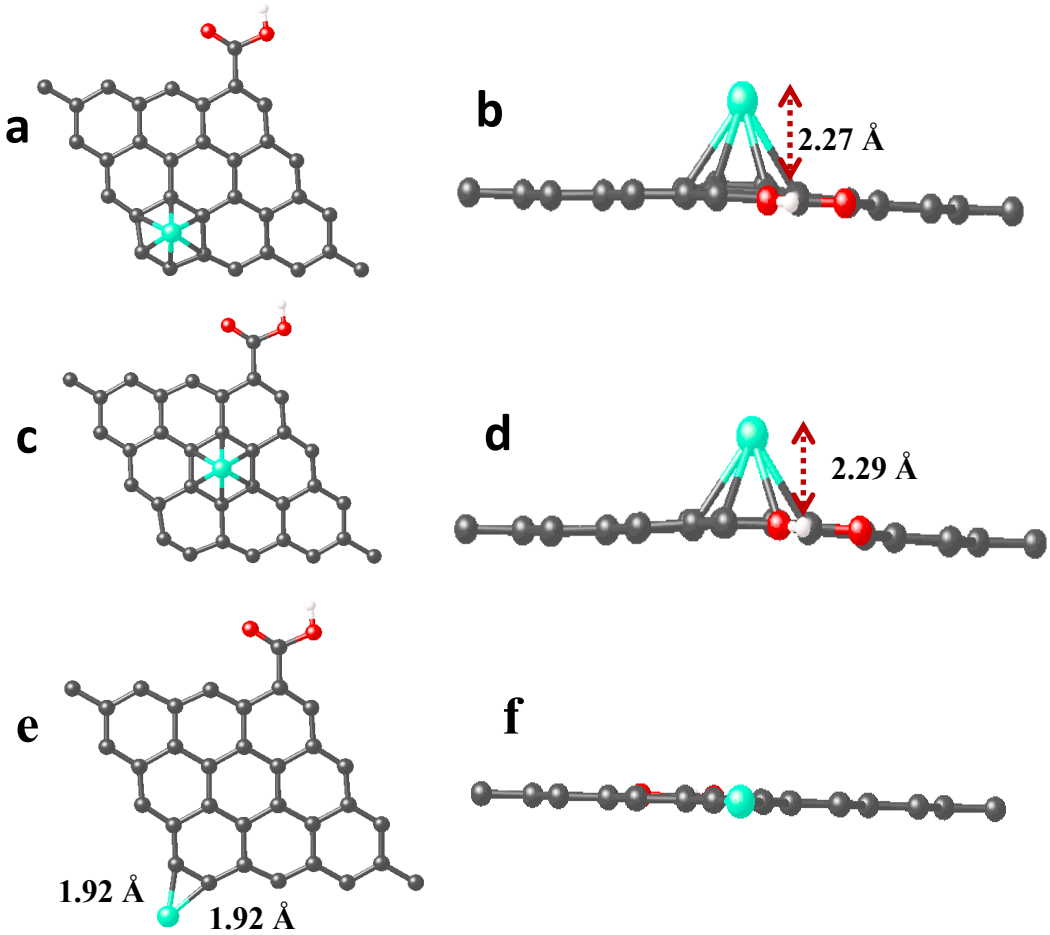

Figure S15. Optimized structure of COOH functionalized GQD-Fe^{3+} complex, (a) bridge-hollow (BH) configuration, (c) hollow-hollow (HH) configuration and (e) Edge-Edge (EE) configuration. (b), (d) & (f) are the side views of the optimized structures presented in (a), (c) & (e), respectively. The carbon, oxygen, hydrogen atoms and Fe^{3+} ion are black, red, pink and green in color, respectively.

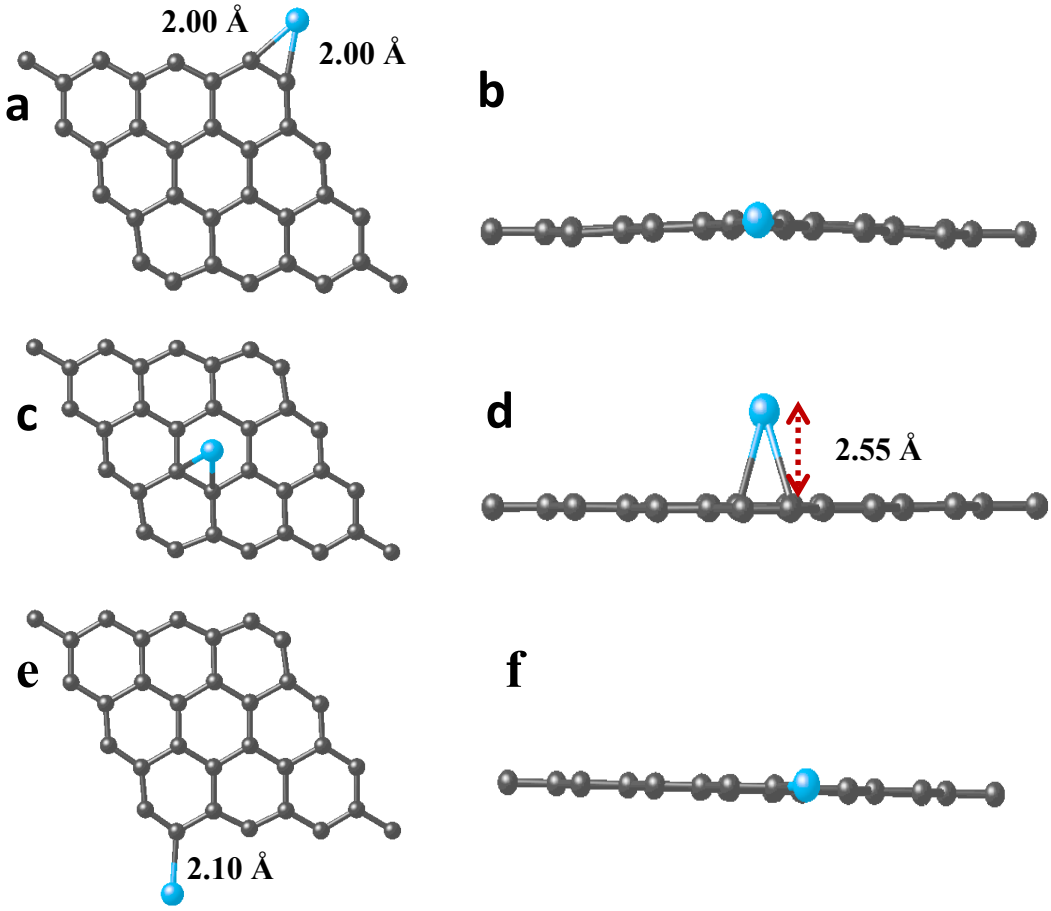

Figure S16. Optimized structure of GQD-Cr complex, (a) bridge-edge (BE) configuration, (c) hollow-hollow (HH) configuration and (e) Edge-Edge (EE) configuration. (b), (d) & (f) are the side views of the optimized structures presented in (a), (c) & (e), respectively. The carbon and Cr atoms are black and blue in color, respectively.

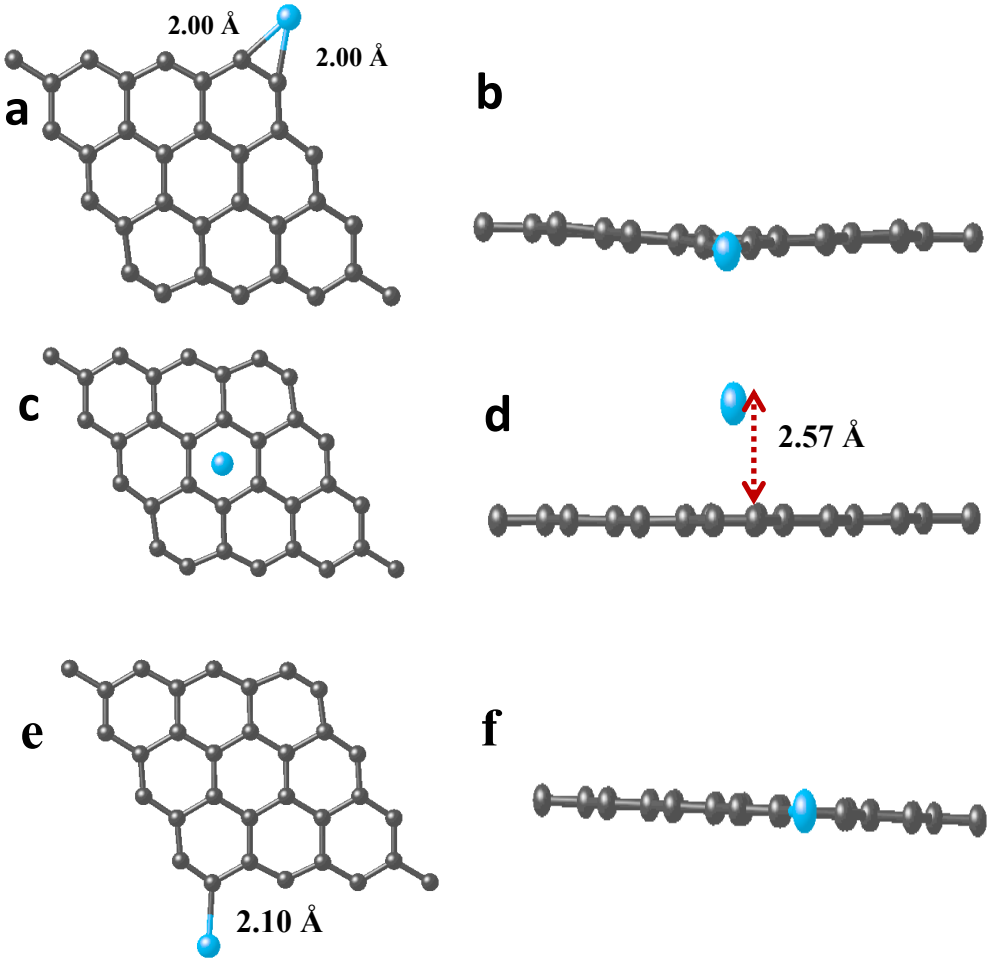

Figure S17. Optimized structure of GQD-Cr^{3+} complex, (a) bridge-edge (BE) configuration, (c) hollow-hollow (HH) configuration and (e) Edge-Edge (EE) configuration. (b), (d) & (f) are the side views of the optimized structures presented in (a), (c) & (e), respectively. The Carbon and Cr^{3+} ion are black and blue in color respectively.

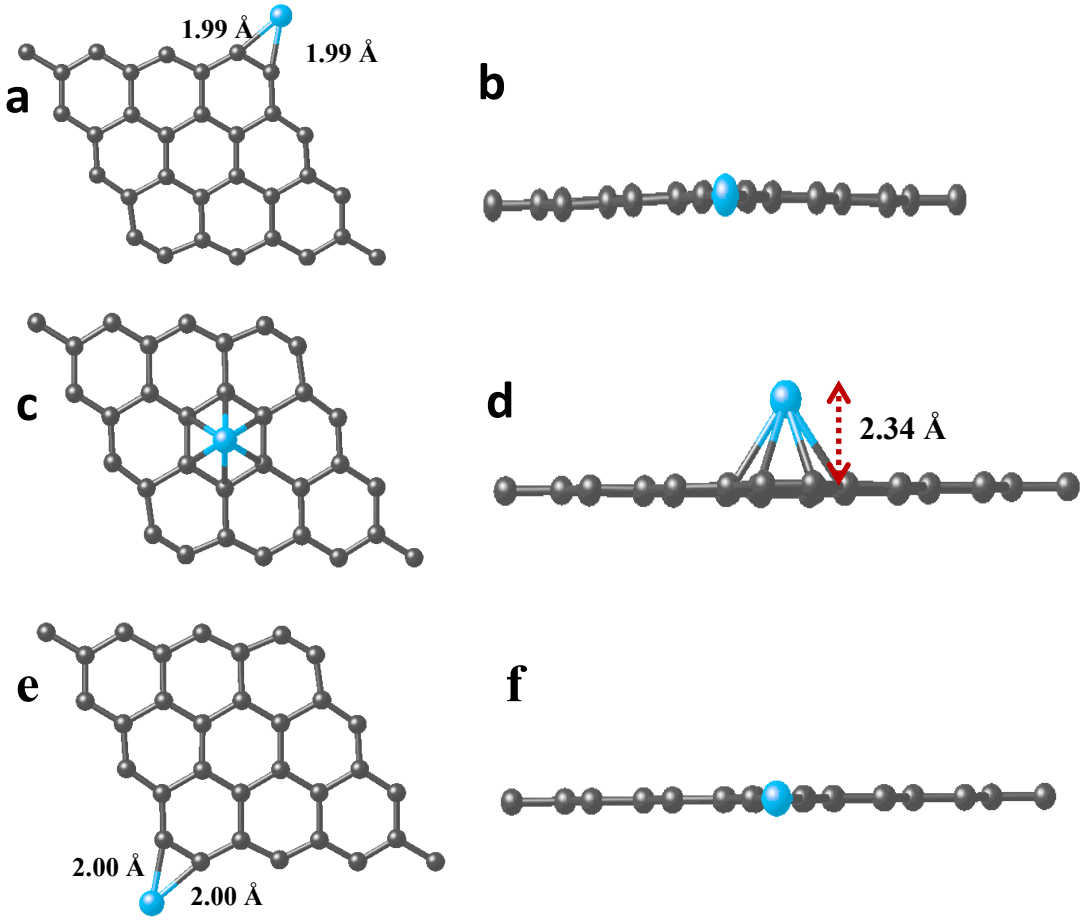

Figure S18. Optimized structure of GQD-Cr^{6+} complex, (a) bridge-edge (BE) configuration, (c) hollow-hollow (HH) configuration and (e) Edge-Edge (EE) configuration. (b), (d) & (f) are the side views of the optimized structures presented in (a), (c) & (e), respectively. The Carbon and Cr^{3+} ion are black and blue in color, respectively.

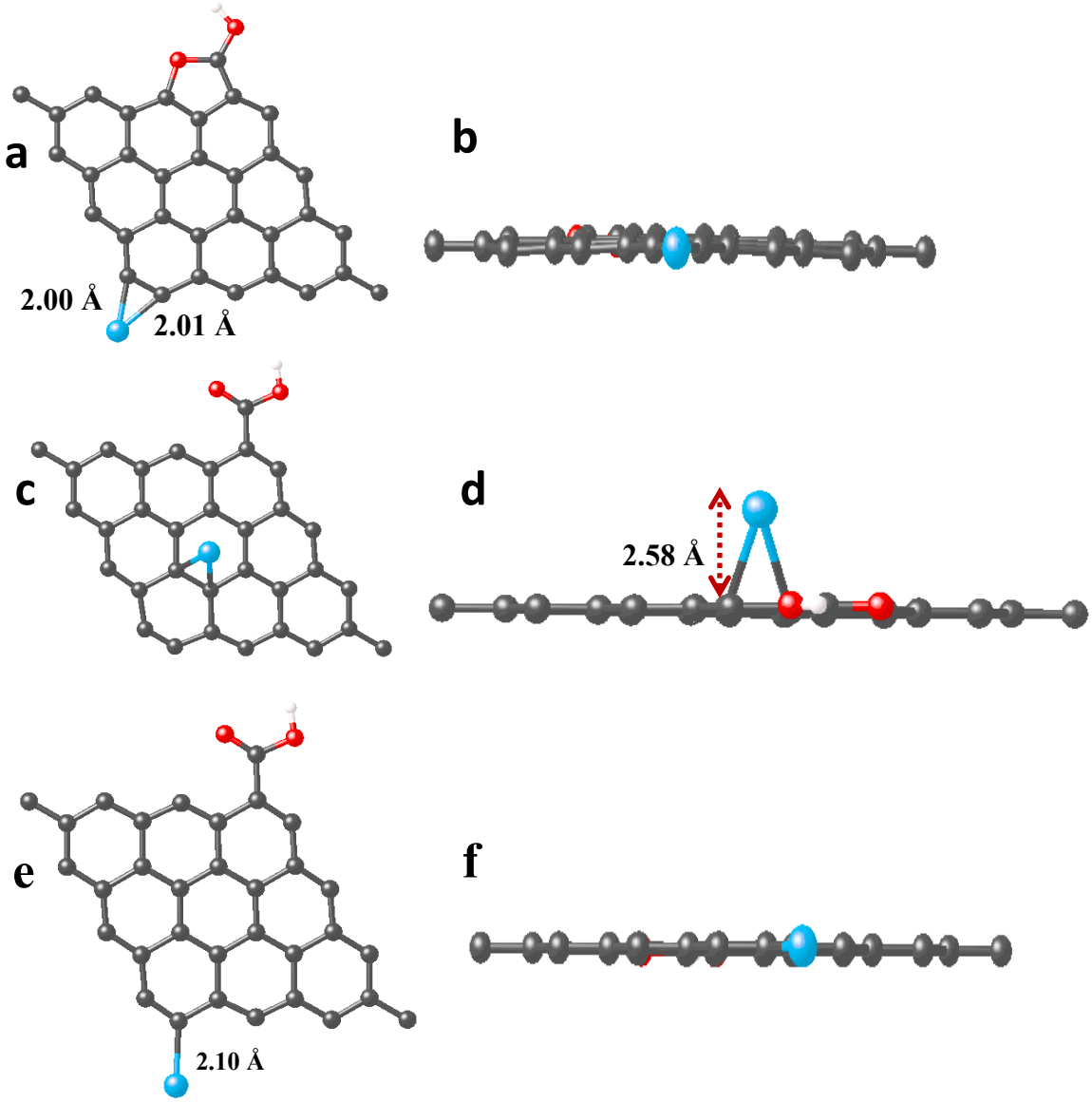

Figure S19. Optimized structure of COOH functionalized GQD-Cr complex, (a) bridge-edge (BE) configuration, (c) hollow-hollow (HH) configuration and (e) Edge-Edge (EE) configuration. (b), (d) & (f) are the side views of the optimized structures presented in (a), (c) & (e), respectively. The carbon, oxygen, hydrogen and Cr atoms are in black, red, pink and blue in color, respectively.

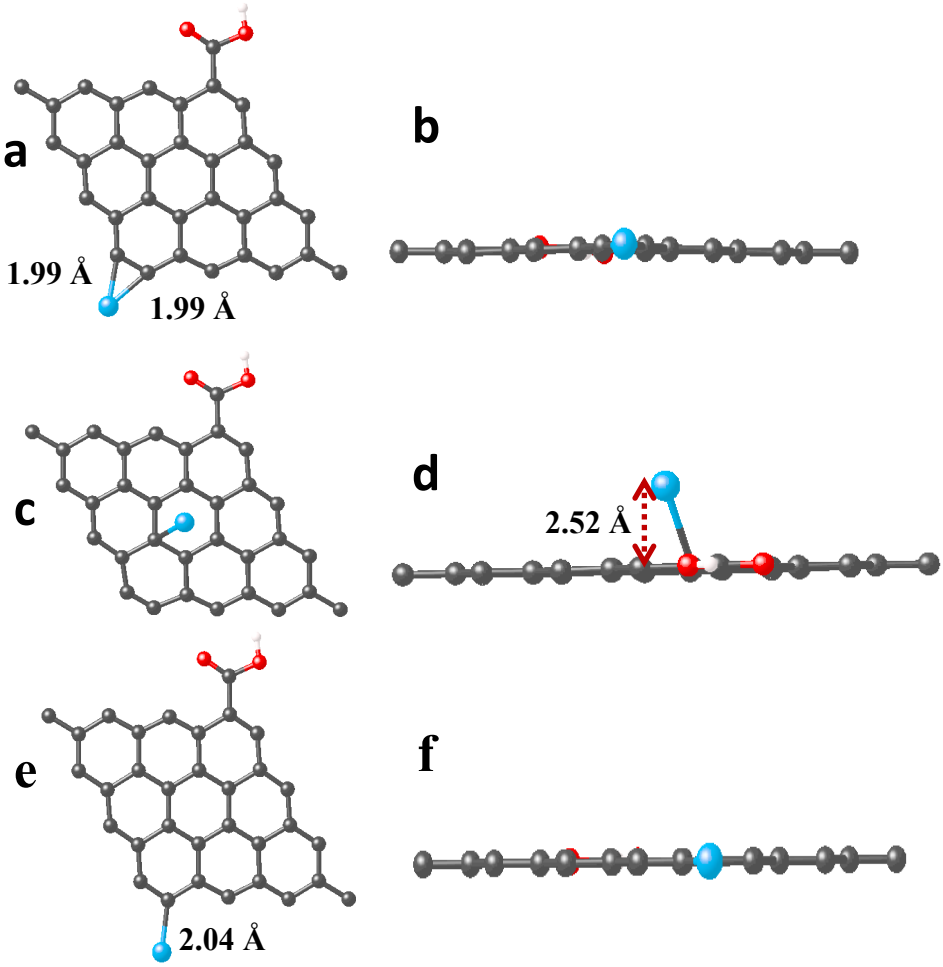

Figure S20. Optimized structure of COOH functionalized GQD-Cr^{3+} complex, (a) bridge-edge (BE) configuration, (c) hollow-hollow (HH) configuration and (e) Edge-Edge (EE) configuration. (b), (d) & (f) are the side views of the optimized structures presented in (a), (c) & (e), respectively. The carbon, oxygen, hydrogen and Cr atoms are in black, red, pink and blue in color, respectively.

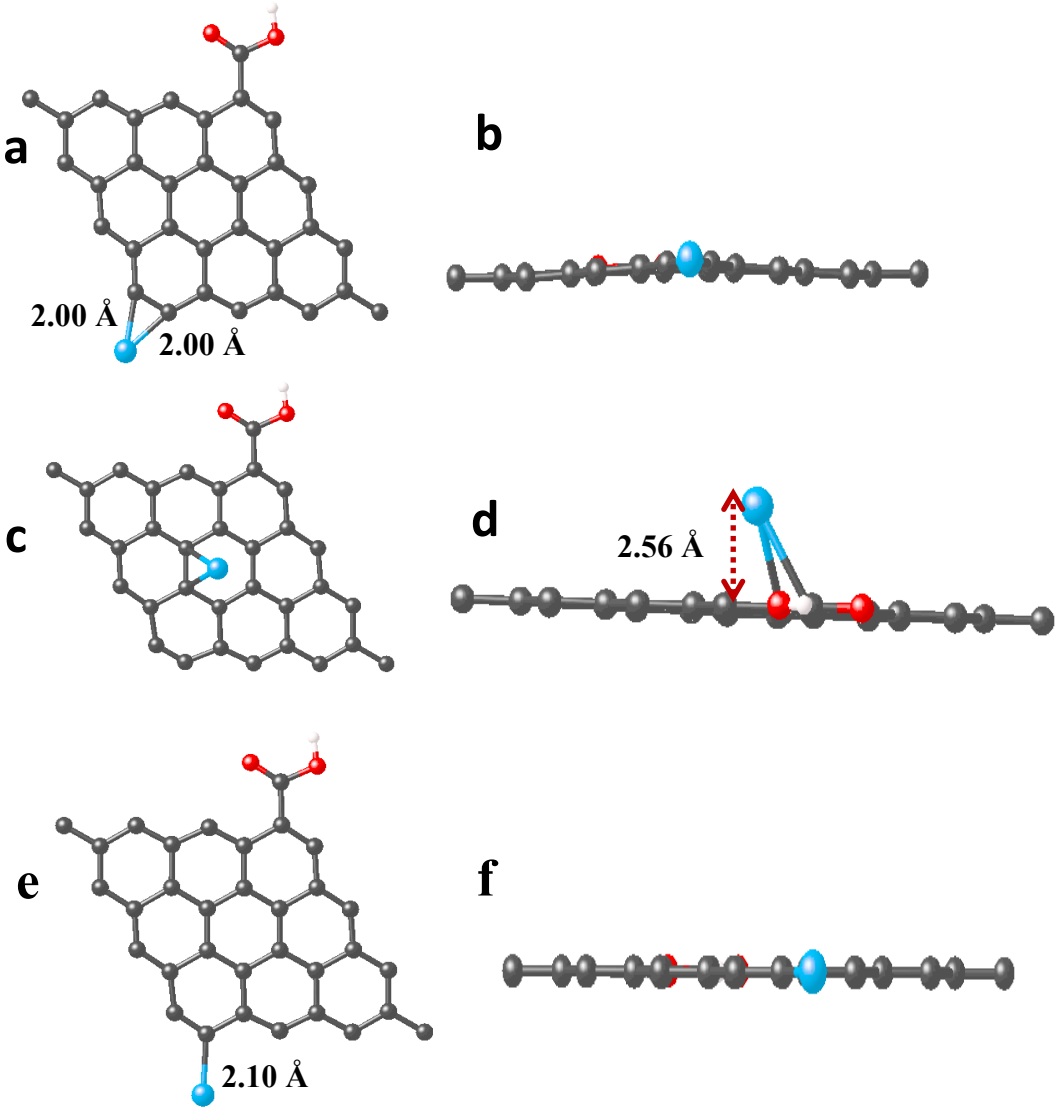

Figure S21. Optimized structure of COOH functionalized GQD-Cr^{6+} complex, (a) bridge-edge (BE) configuration, (c) hollow-hollow (HH) configuration and (e) Edge-Edge (EE) configuration. (b), (d) & (f) are the side views of the optimized structures presented in (a), (c) & (e), respectively. The carbon, oxygen, hydrogen and Cr atoms are in black, red, pink and blue in color, respectively.

References:

1 S. Cao, J. Zheng, J. Zhao, Z. Yang, C. Li, X. Guan, W. Yang, M. Shang and T. Wu, *ACS Appl. Mater. Interfaces*, 2017, **9**, 15605–15614.

2 L. R. De Jesus, R. V Dennis, S. W. Depner, C. Jaye, D. A. Fischer and S. Banerjee, *J. Phys. Chem. Lett.*, 2013, **4**, 3144–3151.

3 V. Lee, R. V Dennis, B. J. Schultz, C. Jaye, D. A. Fischer and S. Banerjee, *J. Phys. Chem. C*, 2012, **116**, 20591–20599.

4 W. Liu, H. Diao, H. Chang, H. Wang, T. Li and W. Wei, *Sensors Actuators, B Chem.*, 2017, **241**, 190–198.

5 J. Shen, S. Shang, X. Chen, D. Wang and Y. Cai, *Mater. Sci. Eng. C*, 2017, **76**, 856–864.

6 Q. Huang, Q. Li, Y. Chen, L. Tong, X. Lin, J. Zhu and Q. Tong, *Sensors Actuators, B Chem.*, 2018, **276**, 82–88.

7 Y. Guo, F. Cao and Y. Li, *Sensors Actuators, B Chem.*, 2018, **255**, 1105–1111.

8 X. Cui, Y. Wang, J. Liu, Q. Yang, B. Zhang, Y. Gao, Y. Wang and G. Lu, *Sensors Actuators, B Chem.*, 2017, **242**, 1272–1280.

9 R. Wang, X. Wang and Y. Sun, *Sensors Actuators, B Chem.*, 2017, **241**, 73–79.

10 R. Atchudan, T. N. J. I. Edison, D. Chakradhar, S. Perumal, J. J. Shim and Y. R. Lee, *Sensors Actuators, B Chem.*, 2017, **246**, 497–509.

11 W. U. Khan, D. Wang, W. Zhang, Z. Tang, X. Ma, X. Ding, S. Du and Y. Wang, *Sci. Rep.*, 2017, **7**, 1–9.

12 H. Xu, S. Zhou, L. Xiao, H. Wang, S. Li and Q. Yuan, *J. Mater. Chem. C*, 2015, **3**, 291–297.

13 R. Guo, S. Zhou, Y. Li, X. Li, L. Fan and N. H. Voelcker, *ACS Appl. Mater. Interfaces*, 2015, **7**, 23958–23966.

14 A. Ananthanarayanan, X. Wang, P. Routh, B. Sana, S. Lim, D. H. Kim, K. H. Lim, J. Li and P. Chen, *Adv. Funct. Mater.*, 2014, **24**, 3021–3026.

15 L. Bu, J. Peng, H. Peng, S. Liu, H. Xiao, D. Liu, Z. Pan, Y. Chen, F. Chen and Y. He, *RSC Adv.*, 2016, **6**, 95469–95475.

16 K. M. Tripathi, A. Singh, A. Bhati, S. Sarkar and S. K. Sonkar, *ACS Sustain. Chem. Eng.*, 2016, **4**, 6399–6408.

17 M. Zheng, Z. Xie, D. Qu, D. Li, P. Du, X. Jing and Z. Sun, *ACS Appl. Mater. Interfaces*, 2013, **5**, 13242–13247.

18 S. Huang, H. Qiu, F. Zhu, S. Lu and Q. Xiao, *Microchim. Acta*, 2015, **182**, 1723–1731.